Structure of Membrane Surfactant and Liquid Crystalline Smectic Lamellar Phases Under Flow

Cyrus R. Safinya, Eric B. Sirota, Robijn F. Bruinsma, Claus Jeppesen, Robert J. Plano, Lawrence J. Wenzel

Science, New Series, Volume 261, Issue 5121 (Jul. 30, 1993), 588-591.

16. R. Bilewicz and M. Majda, *Langmuir* **7**, 2794 (1991).
17. B. Tieke *et al.*, *Colloid Polym. Sci.* **255**, 36 (1977).
18. D. Day and H. Ringsdorf, *J. Polym. Sci. Polym. Lett. Ed.* **16**, 205 (1978).
19. N. Mino, H. Tamura, K. Ogawa, *Langmuir* **8**, 594 (1992).
20. R. R. Chance, G. N. Patel, J. D. Witt, *J. Chem. Phys.* **71**, 206 (1979).
21. M. Shibata, F. Kaneko, M. Aketagawa, S. Kobayashi, *Thin Solid Films* **179**, 433 (1989).
22. F. Kaneko, M. Shibata, S. Kobayashi, *ibid.* **210**, 548 (1992).
23. G. M. Air and W. G. Laver, *Proteins* **6**, 341 (1989).
24. W. Spevak *et al.*, *J. Am. Chem. Soc.* **115**, 1146 (1993).
25. We have previously shown that 1 to 5% of sialoside lipid gives maximum binding of the virus to polymerized liposomes (*24*). Ideal mixing of the two components was determined by analysis of the Langmuir isotherms. Various ratios of monomers **1** and **2** give isotherms whose limiting areas and collapse pressures change in direct proportion to the mole fraction of **2** as expected for miscibility [see (*3*)].
26. R. Maoz and J. Sagiv, *J. Colloid Interface Sci.* **100**, 465 (1984).
27. D. Day and J. B. Lando, *Macromolecules* **13**, 1478 (1980).
28. N. Mino, H. Tamura, K. Ogawa, *Langmuir* **7**, 2336 (1991).
29. M. Wenzel and G. H. Atkinson, *J. Am. Chem. Soc.* **111**, 6123 (1989).
30. G. Lieser, B. Tieke, G. Wegner, *Thin Solid Films* **68**, 77 (1980).
31. R. F. Fischetti, M. Filipkowski, A. F. Garito, J. K. Blaise, *Phys. Rev. B* **37**, 4714 (1988).
32. Expert Committee on Influenza, *WHO Tech. Rep. Ser. No. 64* (1953).
33. T. J. Pritchett, R. Brossmer, U. Rose, J. C. Paulson, *Virology* **160**, 502 (1987).
34. N. K. Sauter *et al.*, *Biochemistry* **28**, 8388 (1989).
35. T. Barrett and S. C. Inglis, in *Virology, A Practical Approach*, B. W. J. Mahy, Ed. (IRL Press, New York, 1985), p. 128.
36. The above experiments define a background level of CR arising from nonspecific adhesion. Thus, from Fig. 4A, the minimum quantity of virus that is detectable and well above this background level is ~25 HAUs. According to some estimates (*35*), this value corresponds to ~200 million particles. Given a cross-sectional area of $\sim 8 \times 10^{-11}$ cm^2 per particle, the minimum film area affected is ~0.02 cm^2, or 1/100 of the sample area. Given the high film response, it is likely that each binding event results in a much longer range induced disorder.
37. We thank M. E. Schaefer and J. H. Gilbert for virus protocols, technical help, and the generous donation of X31 influenza A. Supported by the Director, Office of Energy Research, Office of Basic Energy Sciences, Division of Materials Sciences, and also the Division of Energy Biosciences of the U.S. Department of Energy (DE-AC03-76SF0098). M.D.B. thanks the American Cancer Society for a Junior Faculty Award and Eli Lilly for a Young Investigator Grant. W.S. thanks NIH for a predoctoral training grant. Synthesis of the C-glycoside of sialic acid was supported by the California Competitive Technology Program (grant C89-285) in collaboration with J. R. Murdoch and H. O. Ribi, Biocircuits Corporation.

19 May 1993; accepted 1 July 1993

Structure of Membrane Surfactant and Liquid Crystalline Smectic Lamellar Phases Under Flow

Cyrus R. Safinya,* Eric B. Sirota, Robijn F. Bruinsma, Claus Jeppesen, Robert J. Plano, Lawrence J. Wenzel

Synchrotron x-ray scattering studies were performed to probe the nonequilibrium structures of two layered systems at high shear rates: the smectic-A phase of the thermotropic liquid crystal 4-cyano-4′-octylbiphenyl (8CB) and the lamellar L_α phases of surfactant membranes composed of sodium dodecyl sulfate and pentanol. Whereas the lamellar surfactant phases oriented primarily with their layers parallel to the shearing plates, as expected intuitively, in the corresponding high shear regime, the smectic-A liquid crystalline material oriented with the layers perpendicular to the shearing plates. A careful numerical study revealed that this surprising layer orientation results from nonlinear dynamics of the liquid crystal director and is caused by the flow distortion of thermal fluctuations.

The behavior of relatively simple liquids composed of small molecules, like water, under shear flow is well described by the classical "Newtonian" theory of hydrodynamics (*1*). However, many complex macromolecular fluids, such as lyotropic and thermotropic liquid crystals, colloidal suspensions, and polymeric solutions and melts, have a large-scale interior structure that can be significantly distorted by shear flow because of their relatively long relaxation times (*2*). At the macroscopic level, this distortion manifests itself as a breakdown of Newtonian hydrodynamics that requires the introduction of new stresses in the hydrodynamic equations, so-called "normal stress" effects originally elucidated by Weissenberg in polymeric and surfactant liquids (*3*). The scientific challenge remains to correlate the bulk macroscopic response of the material under stress to the underlying distorted microscopic structure. Non-Newtonian flow behavior in complex fluids plays a central role in the mechanics of many technological materials [for example, in lubricating films (*4*, *5*) and the processing of polymer films and fibers (*6*)], which for the most part occur under poorly understood conditions far from equilibrium. It is precisely in these technologically important materials, which are extremely susceptible to large deformations of their underlying structure (such as layer orientation and macromolecular conformations), that bulk studies with a direct structural probe such as x-rays and neutrons are most relevant.

An important group of complex fluids involves layered materials, which may be used as lubricating films, such as liquid crystals, block copolymers, and surfactant membrane liquids. We focus on experimental results on the dilute lamellar L_α phases of surfactant membranes and on the smectic-A (SmA) phase of liquid crystals composed of rod-like molecules (Fig. 1, A and C) and compare them with results from a numerical study of a simple theoretical model of such materials under conditions of high shear rates. An important advantage of studying these layered systems is that their equilibrium structures have been previously investigated by x-ray scattering (*7*, *8*). The membrane surfaces of the L_α phase were composed of thin water layers coated with surfactant and cosurfactant molecules (SDS and pentanol) separated by dodecane (Fig. 1C). The SmA phase we studied is thermotropic; that is, under heating it transforms into a nematic liquid that has orientational order but no translational order (Fig. 1B) (*9*). We introduce a reduced temperature $t_r = (T - T_{NA})/T_{NA}$, where T_{NA} is the critical temperature for the nematic-SmA transition. Both systems can be viewed as stacks of liquid layers within which the molecules are free to diffuse.

The complex fluids were confined between concentric cylinders transparent to x-rays, with the outer cylinder rotating and the inner fixed, in a specially designed Couette cell (*10*). This approximates a linear velocity (v) profile with a constant shear rate $\gamma = v/D$, where the gap size D was varied between 250 to 2000 μm. The a, b, and c layer orientations, originally introduced by Miesowicz (*11*) to describe flowing nematics, refer to cases with the unit vector normal to the layer $\hat{\mathbf{n}}$ pointing, respectively, along the z, velocity $\mathbf{v}$, and velocity gradient $\nabla\mathbf{v}$ directions (Fig. 2A).

In the lamellar L_α phase, we studied six mixtures with dodecane volume fractions Φ between 0.54 and 0.62, which correspond to multilayer phases with the interlayer spacing d increasing from about 118 to 160 Å (*8*). At high shear rates, the layers were oriented primarily parallel to the shearing plates, as expected intuitively (c orientation). The scattering intensity for a typical

C. R. Safinya, Materials and Physics Departments and the Materials Research Laboratory, University of California, Santa Barbara, CA 93106.
E. B. Sirota and R. J. Plano, Exxon Research and Engineering Company, Annandale, NJ 08801.
R. F. Bruinsma and C. Jeppesen, Physics Department, University of California, Los Angeles, CA 90024.
L. J. Wenzel, American Design Corporation, Stirling, NJ 07980.
*To whom correspondence should be addressed.

L_α sample at $\Phi = 0.58$ with $d = 140$ Å at high shear rates $\gamma = 6000$ Hz (Fig. 2B) shows a peak maximum at scattering vectors $q_{\nabla v} = 2\pi/d = 0.045$ Å^{-1} and $q_z = q_v = 0$ (subscript denotes axis with which the vector component is parallel), which demonstrates that $\hat{\mathbf{n}}$ is along the ∇v direction. As Φ increased from 0.54 to 0.62, the shear rate at which this main orientation was observed decreased from $\gamma \approx 2200$ to 1100 Hz. For low shear rates, at which the formation of spherical, multilayer liposome structures has been observed (*12*), the scattering peak was isotropic, indicative of randomly oriented lamellae.

In the SmA phase, the corresponding behavior was different and quite unexpected. At low shear rates in the smectic phase, the layer normal was found to be distributed nonuniformly about an axis parallel to the flow direction, indicative of a heterogeneously mixed regime of SmA domains with layer orientations between that of the a and c, most likely because of textural patterns reported in earlier microscopy studies of SmA materials under shear flow (*13*). At high shear rates, a pure orientation regime was observed for which the layers orient perpendicular to the shearing plates (a orientation) (*14*). The peak position of the scattering maximum in this regime [for a shear rate of $\gamma = 300$ Hz at $T = T_{NA} - 0.117$°C (Fig. 2C)] is rotated by $\pi/2$ with respect to that of the L_α data. The peak scattering intensity occurs in reciprocal space at a wave vector $q_z = q_0\,\hat{\mathbf{n}}$ with $q_0 = 2\pi/d = 0.198$ Å^{-1} (and $q_{\nabla v} = q_v = 0$),

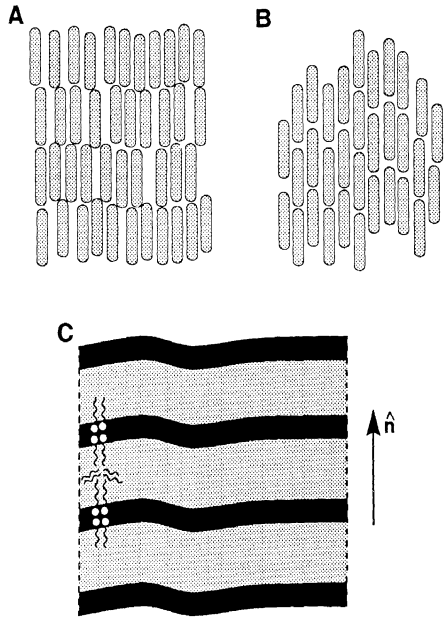

Fig. 1. Schematics of the (**A**) SmA (layered) and the (**B**) nematic phases of rod-shaped liquid crystal molecules. (**C**) Schematic of the layered surfactant membrane L_α phase. The average molecular orientation and the layer-normal directions are specified by the unit vector $\hat{\mathbf{n}}$.

where the SmA layer spacing is $d = 31.73$ Å. In other words, the SmA layers themselves are undergoing constant shear flow, whereas the position of the layer's center of mass does not change. Obviously, only liquid layered systems can do this. The same orientation has recently also been reported for block-copolymer layered materials under shear flow (*15*). A larger shear rate is required for the system to remain in this pure a orientation as the temperature is lowered below T_{NA} into the SmA phase (Fig. 3). The detailed description of the orientational regimes of the nematic phase has been reported elsewhere (*16*).

To obtain insight into this unexpected result of a pure a orientation at high shear rates, we compared the x-ray intensity profile of the SmA phase projected in the shear plane (Fig. 4A) with the profile at a slightly higher temperature $T = T_{NA} + 0.015$°C in the nematic phase (Fig. 4B). There is a close resemblance, except that in the SmA phase the director is more focused along the a orientation. To understand the physics underlying the unusual a orientation, we investigated the nematic phase in the critical regime, the immediate vicinity of T_{NA} where SmA density fluctuations are large. A theoretical description of the nematic phase in the critical regime, both at low (*17*) and high (*18*) shear rates, is available for direct comparison with the experimental results.

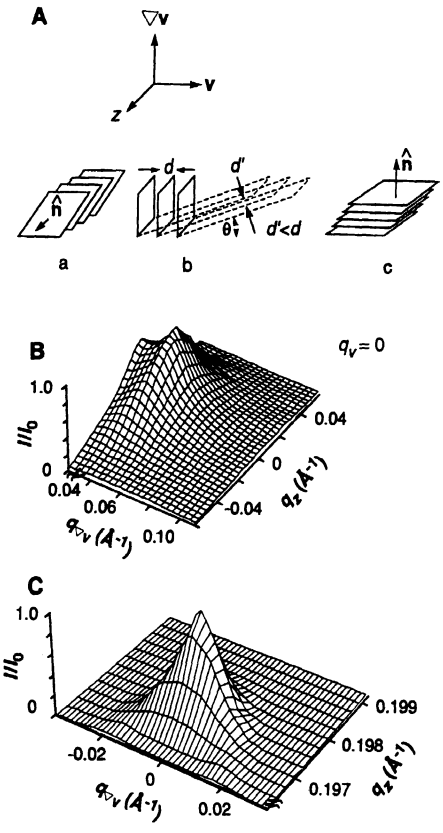

Fig. 2. (**A**) Definition of real-space orientation directions: a, b, and c layer orientations refer to the layer normal $\hat{\mathbf{n}}$ pointing along the *z*, velocity $\mathbf{v}$, and velocity gradient $\nabla\mathbf{v}$ directions, respectively. (**B**) A three-dimensional plot of the x-ray scattering intensity for an L_α membrane multilayer with $\Phi = 0.58$ and $d = 140$ Å under high shear rates ($\gamma = 6000$ Hz) shows a maximum at $q_{\nabla v} = 2\pi/d = 0.045$ Å^{-1} indicative of the intuitive c orientation with the layers sliding over each other. (**C**) Plot of the x-ray data in the SmA phase for a shear rate of $\gamma = 300$ Hz at $T = T_{NA} - 0.117$°C, where the position of the peak (at $q_z = q_0\,\hat{\mathbf{n}}$ with $q_0 = 2\pi/d = 0.198$ Å^{-1} and $q_{\nabla v} = q_v = 0$, with $d = 31.73$ Å) scattering maximum is rotated by $\pi/2$ with respect to that of the L_α data, indicating that the layers assume the unexpected a orientation in parts of the (γ-T) phase diagram (Fig. 3).

In this critical regime, there are long-lived thermal fluctuations (*7*). The dynamics of the director $\hat{\mathbf{n}}$ is controlled by the competition between the viscous torque $\boldsymbol{\Gamma}_v$, caused by the drag of the flowing liquid on the director, and the "smectic" torque $\boldsymbol{\Gamma}_s$, caused by the deformation of these smectic fluctuations by the shear flow. The equation of motion of a spatially uniform (*14*), time-dependent director in the presence of a shear flow $\mathbf{v} = \gamma y\hat{\mathbf{x}}$ (γ is the shear rate) is given by (*9*, *17*)

$$\boldsymbol{\Gamma}_v + \boldsymbol{\Gamma}_s = 0 \qquad (1)$$

The viscous torque is

$$\boldsymbol{\Gamma}_v = -\hat{\mathbf{n}} \times \left[\gamma_1 \frac{\partial \hat{\mathbf{n}}}{\partial t} + \gamma(\alpha_2 n_{\nabla v}, \alpha_3 n_v, 0)\right] \qquad (2)$$

where $n_{\nabla v} = n_y$; $n_v = n_x$; and α_2, α_3 (both negative), and γ_1 are viscosity parameters whose magnitudes can be measured by viscosity studies deep in the nematic phase (*19*). The smectic torque is $\boldsymbol{\Gamma}_s = -\hat{\mathbf{n}} \times \mathbf{h}_s$, where $\mathbf{h}_s$ is the "molecular field" (*9*). For $\hat{\mathbf{n}}$ close to the z axis, $\mathbf{h}_s$ is of the form (*18*)

$$\mathbf{h}_s = (k_B T/d^2 \xi_\parallel)[-(\pi/2) De\, n_x \hat{\mathbf{y}} - 0.13(De)^2 n_x^2 \hat{\mathbf{x}} + O(\gamma\tau)^3 \cdots] \qquad (3)$$

with $\xi_\parallel$, the fluctuation correlation length (the SmA domain size) measured along the director, $De = \gamma\tau$, the Deborah number with τ, the domain lifetime, and k_B, the Boltzmann constant. Near T_{NA}, $\xi_\parallel$ diverges as T approaches T_{NA} (*7*), so that both $\tau \sim \xi_\parallel^{3/2}$ and De diverge rapidly.

Equation 1 defines a nonlinear equation

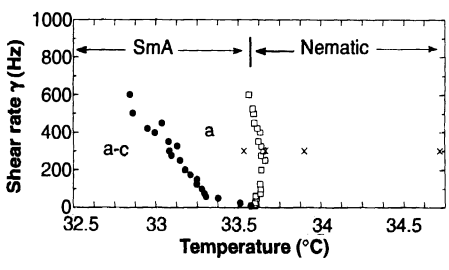

Fig. 3. The shear rate–temperature phase diagram ($T_{NA} = 33.58$°C at zero shear) in the SmA phase showing the pure a and the mixed a-c layer orientation regimes. Crosses mark where the scattering data are shown in Figs. 2, 4, and 5.

of motion for $\hat{n}$ whose solution can be obtained numerically (with use of the complete expression for the molecular field). A noise term was added to Eq. 1 that simulated the mechanical and hydrodynamical noise inside the shear cell. The viscosity parameters and critical temperature were assigned to be their experimental values, and the noise amplitude was treated as a temperature-independent fitting parameter (*20*). The numerical results of the distribution of the nematic director projected in the shear plane just above the transition at $t_r = 0.00005$ and $\gamma = 300$ Hz (Fig. 4C) can be compared directly with the x-ray scattering data at the same t_r (Fig. 4B), which actually provides a direct map of the time-averaged distribution of $\hat{n}$ (*21*). The numerical model and the x-ray data agree quite reasonably, both revealing a highly anisotropic distribution of $\hat{n}$ in the shear plane (elongated along ∇v).

As a check of the model, we collected data at two higher temperatures (t_r = 0.00082 and 0.0035) (Fig. 5A) at which the structure factor was experimentally found to have undergone drastic shape changes compared with the data at t_r = 0.00005. The numerically obtained distributions of $\hat{n}$ (Fig. 5B) show the same rearrangements as the scattering data; therefore, we can be confident that we have an adequate theoretical description of the director dynamics. In particular, both the data and the numerical results show a rotation through $\pi/2$ when temperature is increased so that the director distribution is elongated along the flow.

We can now analyze Eq. 1 to identify the origin of the a orientation. Far above T_{NA}, where $De = \gamma\tau$ is very small, we can set $\mathbf{h}_s = 0$ and analytically solve for $\mathbf{\Gamma}_v = 0$. Provided $\alpha_2\alpha_3$ is positive, as is indeed known to be the case (*19*), one finds flow alignment; that is, $\hat{n}$ points almost along the flow direction corresponding to the b orientation. This orientation has been experimentally observed (*16, 19*). As we approach T_{NA}, τ starts to grow and $\mathbf{h}_s$ becomes appreciable. However, as long as *De* is small compared with 1, we need only retain the first-order term of $\mathbf{h}_s$. This term can be absorbed by a redefinition of the α_3 viscosity parameter (*17, 18*) as

$$\alpha_3^R = \alpha_3 + (\pi/2)(k_BT/d^2)(\tau/\xi_\parallel) \qquad (4)$$

and we can continue to use $\mathbf{\Gamma}_v = 0$. As τ grows, α_3^R becomes positive, as is seen experimentally (*19*). We then lose the static solution: For $\alpha_2\alpha_3^R < 0$, one only finds precessing solutions (*18*) with the director moving over a distorted cone [with $(n_{\nabla v}/n_v)^2 = (\alpha_3^R/|\alpha_2|)$] centered about the z axis with a precession frequency $\omega_0 = \gamma(-\alpha_2\alpha_3^R)^{1/2}/\gamma_1$. Except close to T_{NA}, ω_0 is of order γ. As an example, when t_r = 0.0008, $-\alpha_2 \approx \alpha_3^R$ (Fig. 5). The equation of motion $\mathbf{\Gamma}_v = 0$ predicts that the director should move on a cone (with $n_{\nabla v} \approx n_v$). Both the numerical and experimental results are indeed consistent with uniform precession and a slow, noise-induced drift of the apex angle.

For t_r = 0.00005 in Fig. 4, B and C, *De* is of order 1, and we must include the second-order term of $\mathbf{h}_s$ given by Eq. 3. Analytical study of Eq. 1 (*18*) shows that it predicts (i) that the motion of the director should be strongly confined to the z-∇v plane and (ii) that the precessional motion is damped; that is, the director slowly falls toward the z axis or a orientation with a damping time

$$T_1^{-1} = 0.13(k_BT/\gamma_1 d^2\xi_\parallel)(\gamma\tau)^2 \qquad (5)$$

For large t_r, T_1^{-1} is small compared with ω_0, but for t_r = 0.00005, $T_1^{-1} \sim \omega_0 \sim 10$ Hz for γ = 300 Hz, so the motion is overdamped and the director assumes the a orientation.

The second-order term of $\mathbf{h}_s$ (Eq. 3) is thus responsible for the layer orientation. Physically, this means that the a orientation is assumed because it minimizes the elastic deformation energy by flow of thermal fluctuations (*18*). This term is actually a "normal stress" effect similar to that encountered in polymer liquids (*2, 3*). Because both nematic data (Fig. 4B) and SmA data (Fig. 4A) show the same behavior focused along the z axis with an anisotropic distribution in the shear plane, we believe that an analogous explanation holds on the SmA side as well, where it is well known that large critical fluctuations are exhibited (*7*). However, there is at present no theory that can predict how deep we can enter the SmA phase and still have enough critical fluctuations to provide the a orientation or whether the noncritical but long-lived layer undulation fluctuations of the SmA phase can play an analogous role.

The majority of experimental work on flowing complex fluids has emphasized mac-

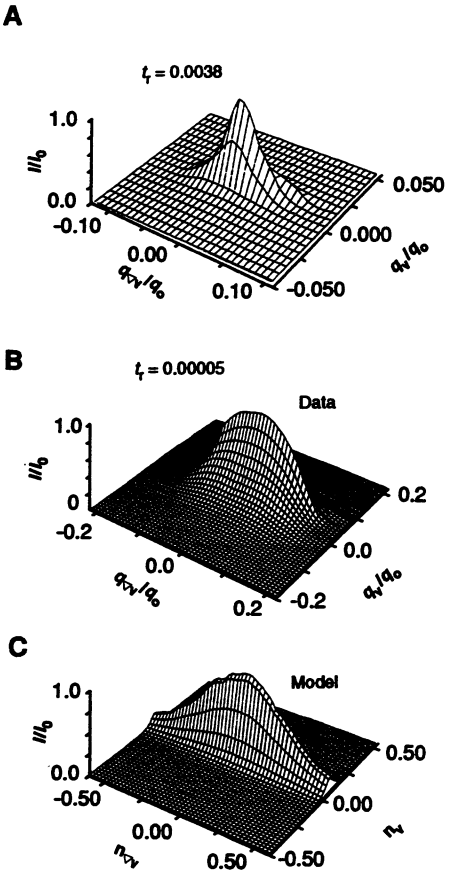

Fig. 4. The x-ray scattering profile and results of the numerical model projected in the $(q_{\nabla v}$-$q_v)$ shear plane. (**A**) The SmA phase scattering data of Fig. 2C. (**B**) The nematic phase data just above the transition at $T = T_{NA}$ + 0.015°C (t_r = 0.00005) at a shear rate of 300 Hz. (**C**) Numerical results of the distribution of the nematic director projected in the shear plane at the same reduced temperature of the nematic phase data.

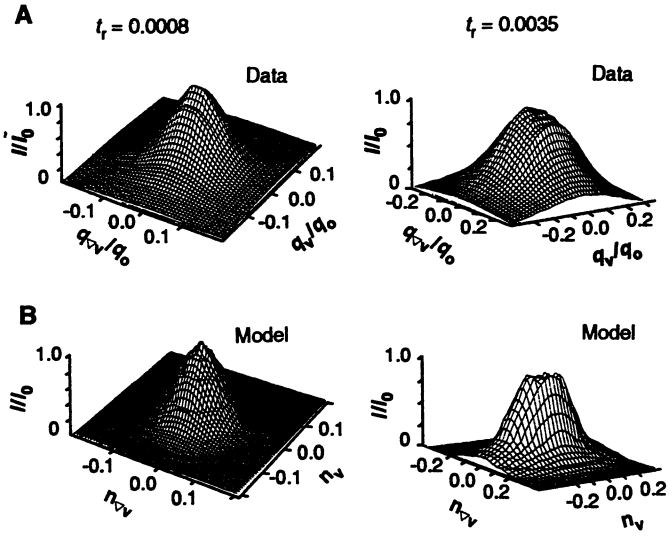

Fig. 5. (**A**) The x-ray scattering profiles projected in the $(q_{\nabla v}$-$q_v)$ shear plane and (**B**) the results of the corresponding numerical model of the distribution of the nematic director at the reduced temperatures t_r = 0.00082 and 0.0035. Both show the evolution in the shapes of the anisotropic profiles as discussed in the text.

roscopic rheological parameters, such as viscosity and normal stress measured either for large (*3*, *4*) or small (*5*) gaps. Our results show the crucial importance of a direct structural probe, such as synchrotron x-ray scattering, in the elucidation of the microstructure that underlies the macroscopic rheological shear and normal stress responses of flowing complex fluids.

REFERENCES AND NOTES

1. G. K. Batchelor, *An Introduction to Fluid Dynamics* (Cambridge Univ. Press, Cambridge, 1970).
2. See, for example, P. G. de Gennes, *Scaling Concepts in Polymer Physics* (Cornell Univ. Press, Ithaca, NY, 1979); S. A. Safran and N. A. Clark, Eds., *Physics of Complex and Supermolecular Fluids* (Wiley, New York, 1987); C. R. Safinya, S. A. Safran, P. A. Pincus, Eds., *Macromolecular Liquids*, vol. 177 of *Materials Research Society Symposium Proceedings* (Materials Research Society, Pittsburgh, PA, 1990).
3. K. Weissenberg, *Nature* **159**, 310 (1947).
4. P. Oswald and M. Kleman, *J. Phys. (Paris) Lett.* **43**, 411 (1982); T. E. Fischer, S. Bhattacharya, R. Salher, J. L. Lauer, Y.-J. Ahn, *Tribol. Trans.* **31**, 442 (1988).
5. J. N. Israelachvili, P. M. McGuiggan, A. M. Homola, *Science* **240**, 189 (1988); J. Van Alsten and S. Granick, *Phys. Rev. Lett.* **61**, 2570 (1988); J. Klein, D. Perahia, S. Warburg, *Nature* **352**, 143 (1991).
6. J. R. A. Pearson, in *Mechanics of Polymer Processing* (Elsevier, London, 1985).
7. J. D. Litster and R. J. Birgeneau, *Phys. Today* **35** (no. 5), 26 (1982); P. S. Pershan, *Structure of Liquid Crystal Phases* (World Scientific, Singapore, 1988); D. Davidov *et al.*, *Phys. Rev. B* **19**, 1657 (1979).
8. C. R. Safinya *et al.*, *Phys. Rev. Lett.* **57**, 2718 (1986); C. R. Safinya, E. B. Sirota, D. Roux, G. S. Smith, *ibid.* **62**, 1134 (1989); G. S. Smith, E. B. Sirota, C. R. Safinya, R. J. Plano, N. A. Clark, *J. Chem. Phys.* **92**, 4519 (1990); D. Roux, C. R. Safinya, F. Nallet, in *Modern Amphiphilic Physics*, A. Ben-Shaul, W. Gelbart, D. Roux, Eds. (Springer, New York, in press).
9. P. G. de Gennes, *The Physics of Liquid Crystals* (Oxford Univ. Press, London, 1974).
10. R. J. Plano, C. R. Safinya, E. B. Sirota, L. Wenzel, *Rev. Sci. Instrum.* **64**, 1309 (1993).
11. M. Miecowicz, *Nature* **158**, 27 (1946).
12. O. Diat and D. Roux, *J. Phys. (Paris)*, in press.
13. R. G. Horn and M. Kleman, *Ann. Phys. (Paris)* **3**, 229 (1978); R. Ribotta and G. Durand, *J. Phys. (Paris)* **38**, 179 (1977).
14. In the high-shear regime, the elastic torque attributable to the spatial dependence of the director, because of textural defects or boundary conditions or both, can be neglected as described in (*9*, *17*).
15. K. A. Koppi, M. Tirrell, F. S. Bates, K. Almdal, R. H. Colby, *J. Phys.* (Paris) **2**, 1941 (1992); K. A. Koppi, M. Tirrell, F. S. Bates, *Phys. Rev. Lett.* **70**, 1449 (1993).
16. C. R. Safinya, E. B. Sirota, R. Plano, R. Bruinsma, *J. Phys. Condens. Matter* **2**, SA365 (1990); C. R. Safinya, E. B. Sirota, R. Plano, *Phys. Rev. Lett.* **66**, 1986 (1991).
17. W. L. McMillan, *Phys. Rev. A* **9**, 1720 (1974); F. Janig and F. Brochard, *J. Phys. (Paris)* **35**, 301 (1974).
18. R. F. Bruinsma and C. R. Safinya, *Phys. Rev. A* **43**, 5377 (1991).
19. P. Pieranski and E. Guyon, *Phys. Rev. Lett.* **32**, 924 (1974); K. Skarp *et al.*, *Mol. Cryst. Liq. Cryst.* **66**, 199 (1981).
20. To fix $De = \gamma\tau$ for the numerical runs, we determined the fluctuation relaxation time $\tau = (2/\pi)(\alpha_3^R - \alpha_3)(\xi_\parallel d^2/k_B T)$ using the experimental data: (i) $\alpha_3^R/|\alpha_2| = (n_{\nabla v}/n_v)^2$, the ratio of the widths of the x-ray data measured in the nematic phase along the ∇v and v directions [described in (*16*)]; (ii) in 8CB, $|\alpha_2| \approx 3$ poise, independent of T (*19*); and (iii) the measured equilibrium value of $\xi_\parallel(t)$ for 8CB was used (*7*).
21. We note that for an arbitrary orientation of $\hat{n}$, the corresponding scattering spot points along $\hat{n}$ and occurs at $\mathbf{q} = q_0\hat{n}$ in reciprocal space. Thus, an anisotropic (isotropic) distribution of $\hat{n}$ about the z axis would result in a corresponding anisotropic (or isotropic) scattering "patch" on a sphere of radius q_0 centered about the q_z axis.

22. We gratefully acknowledge conversations with R. Larson, J. Prost, D. Roux, and, in particular, J. Israelachvili and T. Witten. Synchrotron x-ray scattering experiments carried out on beam line X-10A at the National Synchrotron Light Source at the Brookhaven National Laboratories, which is supported by the U.S. Department of Energy. The Materials Research Laboratory at Santa Barbara is supported by National Science Foundation grant DMR-9123048. Supported in part by Office of Naval Research grant N00014-93-1-0269 (C.R.S.).

6 April 1993; accepted 4 June 1993

Relation of Major Volcanic Center Concentration on Venus to Global Tectonic Patterns

L. S. Crumpler, James W. Head, Jayne C. Aubele

Global analysis of NASA Magellan image data indicates that a major concentration of volcanic centers covering ~40 percent of the surface of Venus occurs between the Beta, Atla, and Themis regiones. Associated with this enhanced concentration are geological characteristics commonly interpreted as rifting and mantle upwelling. Interconnected low plains in an annulus around this concentration are characterized by crustal shortening and infrequent volcanic centers that may represent sites of mantle return flow and net downwelling. Together, these observations suggest the existence of relatively simple, large-scale patterns of mantle circulation similar to those associated with concentrations of intraplate volcanism on Earth.

Detailed volcanological observations of the surface of Venus that are necessary to address fundamental questions about its geological comparisons with Earth are now possible with Magellan synthetic aperture and altimetry radar data (*1*). Here, we concentrate on the distribution of these volcanic centers, their correlation with global geological characteristics, and the possible origin of these global characteristics through large-scale mantle anomalies and dynamic patterns.

The initial analysis of Magellan data resulted in the identification, description, and location, to the nearest half-degree, of 1662 individual volcanic centers and related features larger than 20 km in diameter (*2*–*5*). On the basis of the resulting global distribution map (Fig. 1A), volcanic centers >20 km in diameter are not randomly distributed but are instead concentrated in certain specific regions. This pattern is in contrast to that for impact craters on Venus, the distribution of which cannot be distinguished from that expected for a completely spatially random case (*6*). However, volcanic centers are not arranged in linear patterns as are plate boundary volcanoes on Earth. In this respect and in terms of the estimated global volume flux (<1 km^3 per year) of associated volcanism (*2*), they are comparable to intraplate volcanism (hot spots) on Earth.

Department of Geological Sciences, Brown University, Providence, RI 02912.

Areas over which the concentration of volcanic centers exceeds the global mean density (3.5 ± 2.9 centers per 10^6 km^2) by at least 2σ vary in width from a few hundred to a few thousand kilometers in diameter over physiographically well defined areas (Fig. 1B). An equidimensional region ~13,000 km in diameter of moderate to high areal abundance of volcanic centers (>3 to 7 centers per 10^6 km^2) is centered near the equator at longitude ~250°E between the Beta, Atla, and Themis regiones (BAT). For comparison, the maximum density of hot spot volcanic centers on Earth (*7*) is ~0.1 to 0.2 centers per 10^6 km^2 (*8*). This smaller figure for Earth reflects the relatively younger age of Earth's sea floor (~70 million years) relative to the inferred average surface age (0.5 billion years) of Venus (*9*) and the greater number of volcanic features on Venus, many of which may not be of hot spot origin. Although the BAT anomaly is the largest global concentration, smaller concentrations with similar density occur clustered about the equator in the opposite hemisphere near longitude 70°E. Similar hemispherically symmetric distributions and hemispherically asymmetric concentration levels characterize the distribution of intraplate volcanic centers (hot spots) on Earth (*10*).

The area of the BAT anomaly covers up to ~40% of the global surface, and the density of the volcanic centers exceeds the global mean density over >50% of the surface of Venus. Volcanic centers occur